NANO LETTERS

Letter

pubs.acs.org/NanoLett

Bias-Dependent Molecular-Level Structure of Electrical Double Layer in Ionic Liquid on Graphite

Jennifer M. Black,[†] Deron Walters,[‡] Aleksander Labuda,[‡] Guang Feng,*[,§] Patrick C. Hillesheim,[∥] Sheng Dai,[∥] Peter T. Cummings,[§] Sergei V. Kalinin,[†] Roger Proksch,[‡] and Nina Balke*[,†]

[†]Center for Nanophase Materials Sciences, Oak Ridge National Laboratory, Oak Ridge, Tennessee 37831, United States

[‡]Asylum Research, an Oxford Instruments Company, Santa Barbara, California 93117, United States

[§]Chemical and Biomolecular Engineering, Vanderbilt University, Nashville, Tennessee 37235, United States

[∥]Chemical Sciences Division, Oak Ridge National Laboratory, Oak Ridge, Tennessee 37831, United States

ABSTRACT: Here we report the bias-evolution of the electrical double layer structure of an ionic liquid on highly ordered pyrolytic graphite measured by atomic force microscopy. We observe reconfiguration under applied bias and the orientational transitions in the Stern layer. The synergy between molecular dynamics simulation and experiment provides a comprehensive picture of structural phenomena and long and short-range interactions, which improves our understanding of the mechanism of charge storage on a molecular level.

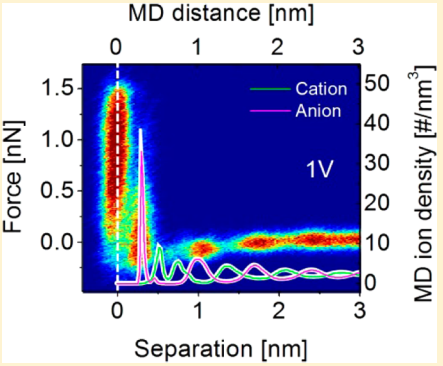

KEYWORDS: *Ionic liquid, highly ordered pyrolytic graphite, electrochemical double layer, atomic force microscopy, force−distance curve*

The structure and properties of solid−liquid interfaces directly underpin the multitude of phenomena in virtually all areas of scientific inquiry ranging from energy storage and conversion systems, biology, to geophysics and geochemistry. These interfaces will affect the lifetimes and stability of batteries, erosion, and corrosion, and many other phenomena. In many cases, the associated mechanisms include the static properties of interfaces, as well as dynamic transport through solid and liquid phases, and electrochemical properties and reactivity, resulting in systems of extreme complexity. However, several broad classes of systems are controlled purely by the structure and dynamics of the electrical double layers (EDL) and the reversible ionic dynamics within.

The paragon of such systems are electrochemical capacitors (ECs) which are capable of very high power density (10 kW kg^{-1}) able to fully charge or discharge in seconds, and as such play an important role in the field of energy storage.[1,2] Compared to batteries, the energy density of ECs is much lower and therefore much effort is directed toward improving the energy density of ECs.[3−9] One strategy is to use ionic liquid (IL) electrolytes, which increase the operational voltage (V), thereby increasing the stored energy (E) according to the equation $E = 1/2CV^2$, where C is capacitance.

For EC applications, highly porous carbon-based materials are typically used as the electrode material with ions from the electrolyte adsorbing and arranging at the carbon surface to form the EDL and balance the electrode charge. The capacitance of ECs is controlled by the EDL structure and the effective pore area, whereas power density is controlled by ionic transport in complex micro/mesoporous systems. The latter has been studied using electrochemical dilatometry for ionic liquids.[10] However, the structure of the EDL on a molecular level and its evolution with bias has been elusive. While significant progress has been achieved based on surface force apparatus,[11−15] scattering,[16,17] and computational methods,[18−24] lateral inhomogeneities of surfaces necessitate spatially resolved methods for local exploration of EDL structure and dynamics. Atomic force microscopy (AFM) force spectroscopy is a technique capable of performing local characterization of the EDL. AFM has been used to probe the structure of various ionic liquids at different interfaces (mica, silica, Au(111) and graphite) by performing force distance (FD) curves.[25−33] Although the role of bias was reported for ionic layering on Au,[26,29] the effect of electrode potential has not been investigated for carbon-based materials.[32] Investigation of the effect of potential on the structure of ionic liquids at carbon interfaces is highly desirable since it will relate to the performance of carbon based ECs using IL electrolytes.

Here we report the bias-evolution of the EDL structure of an ionic liquid on highly ordered pyrolytic graphite (HOPG) as a

Received: August 19, 2013
Revised: November 6, 2013
Published: November 11, 2013

   dx.doi.org/10.1021/nl4031083 | *Nano Lett.* 2013, 13, 5954−5960

model system for carbon-based electrodes for ECs. AFM force spectroscopy is used to measure the ion layering at the electrode surface. One focus of this paper is the statistical reproducibility of the measured FD curves, which is typically neglected in other studies.[25] Matching the experimental data with molecular dynamic (MD) simulations allows us to resolve steric effects. Under bias, we observe the reconstruction of the Stern layer that consists of a reorientation of molecules as evident from MD simulations. In all cases, we observe an excellent agreement between the AFM experiment and MD simulations that allows us to characterize different aspects of the EDL in ionic liquids.

As a model system to explore the structure and properties of the EDL for EC electrodes as a function of applied bias, we have chosen $[Emim^+][Tf_2N^-]$ on HOPG. Figure 1a shows a

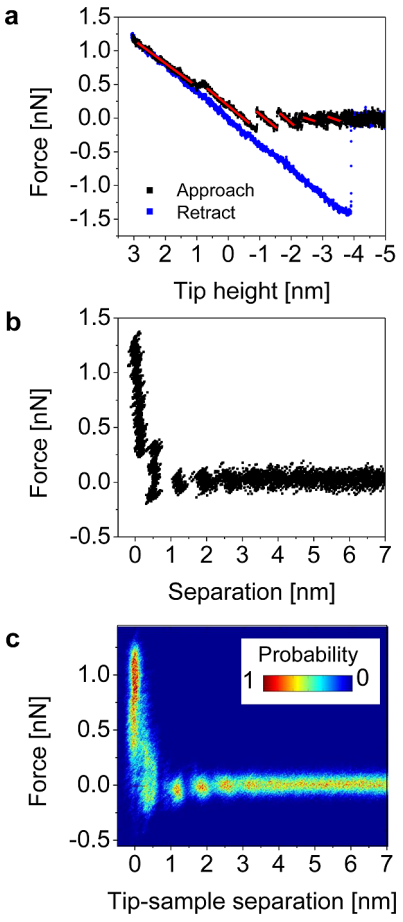

Figure 1. Details of single force–distance curves. (a) Single approach and retract curve showing multiple ion layers. (b) Single force separation plot of curve shown in (a), and 2D histogram of 50 consecutively measured force curves (c).

characteristic force distance curve. During the tip approach, discontinuities (steps) in the force distance curve can be clearly seen before the sample surface is reached (this is when no steps appear even at high forces). These steps are formed by the interaction of the AFM tip and the ion layers at the electrode surface. There may also be ion layers formed at the tip apex, however previous results reported for aqueous systems are controversial.[34,35] An experimental study examining different tip and surface chemistries found structuring at the tip apex does not play a role the measured force–distance curves and suggests that the high local curvature of the AFM tip prevents this structuring.[34] On the other hand, theoretical results predict that water layers are present on the AFM tip and resulting force profiles are a result of merging water layers on the AFM tip and surface.[35] Additional theoretical work has shown that the radius of the tip affects the amplitude of the forces measured but not the step sizes.[36−38] The effects of potential ion layers at the tip apex in ionic liquids are unknown at this point and are being further investigated.

The force from the approach curve in Figure 1a was plotted versus the tip–sample separation (Figure 1b), which is the relevant variable for analyzing the distances between different ionic liquid layers. The first ion layer is approximately 0.37 nm away from the electrode surface. Subsequent ion layers were determined to be approximately 0.7 nm away from each other. Taking into account that the dimensions of the ions are $0.85 \times 0.55 \times 0.28$ nm^3 and $1.09 \times 0.51 \times 0.47$ nm^3 for $[Emim^+]$ and $[Tf_2N^-]$, respectively,[13] it is possible that the measured ion layer size of 0.7 nm could consist of a single ion or a cation–anion pair. Previous work shows that the ions are removed as ion pairs, allowing the system to maintain electroneutrality.[12−15,27,31,32]

In order to investigate the statistical significance of the spacing of the measured ion layers, the two-dimensional (2D) histograms were calculated using 50 measured force distance curves (Figure 1c). The color represents the probability that a point is in the specified sector of the force separation plot. It can be clearly seen that the force separation curves are very reproducible, since the measurements are performed slowly enough to allow reformation of the ion layers between subsequent force curves.

To investigate the change of the ion layering in the EDL when the sample is biased, 1 V and −1 V are applied between sample and conductive tip holder, which is grounded, and in contact with the ionic liquid. For future investigations the authors are developing a three electrode setup to allow for more precise control of the electrode potential. Figure 2 shows the comparison of the extracted 2D histograms of the unbiased and biased HOPG. It can be seen that there are additional ion layers measurable for the biased electrode which are marked in Figure 2 with red arrows. These layers were not visible in the unbiased sample and show only a very low probability. On the right side of Figure 2, data points of the force separation curves with a probability of 50% and higher are shown. We note that the mentioned extra ion layers for the biased electrodes are not present, which means less than 50% of the measured force distance curves show these ion layers. This emphasizes the importance of measuring enough force–distance curves to perform statistical data analysis. However, the first ion layer closest to the electrode surface can be measured very reproducibly for both the unbiased and biased electrodes. For the unbiased case, the first ion layer has a broader distribution compared to the biased cases and consists of two separated sample-ion spacings of 0.3 nm and 0.5 nm. The distance of this ion layer from the sample surface drops for the unbiased sample, to 0.31 nm for 1 V bias and to 0.26 nm for −1 V bias. The measurement of the distance between the ion layers and the sample surface provides direct insight into the charge storage mechanism.

In order to understand the measured steps in the force distance curves and relate them to the ion layering, MD simulations were performed to calculate the cation and anion ordering on graphene surfaces under different voltages. Details

dx.doi.org/10.1021/nl4031083 | Nano Lett. 2013, 13, 5954−5960

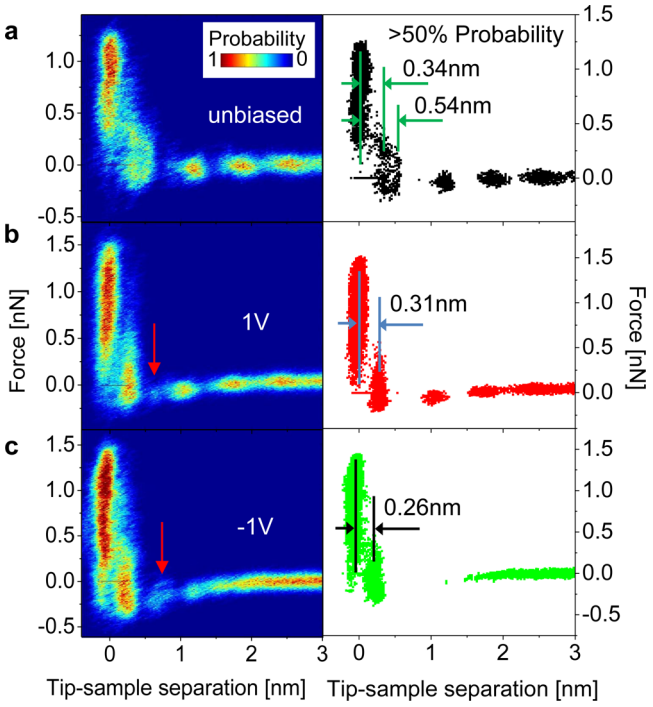

Figure 2. Force-separation plots for unbiased and biased sample. (a) Two-dimensional force separation histogram of 50 consecutively measured force curves (left) and extracted force separation curves with at least 50% probability (right). (b) Two-dimensional force separation histogram of 80 curves and >50% probability points for an applied bias of 1 V and (c) −1 V extracted from 90 force separation curves. The red arrows denote extra steps in the force separation curve for the biased HOPG.

of the simulation can be found in the methods section. Figure 3 shows the ion density distribution as a function of distance from the electrode surface for a potential range of about −2 to 2 V for [Emim$^+$] (Figure 3a) and [Tf_2N^-] (Figure 3b).

The simulation revealed that the EDL consists of a layered structure of cation and anions with cations being closest to the biased surface for negative potentials and anions for positive potentials. The ion density is highest closest to the surface and drops moving further from the surface. The layering of cations and anions was found within 1.5−3 nm from the electrified surfaces under a potential range of about −2 to 2 V which matches the observed layering distance in the force distance curves.

First, we are going to explore the ion layering for the unbiased HOPG surface, that is, at the point of zero charge (PZC). Figure 4a,b displays the anion and cation density distribution together with the experimental data from Figure 2a (>50% probability) for the unbiased electrode, respectively. From the MD simulation, it can be seen that the first ion layer closest to the sample surface (<0.65 nm) consists of two densely spaced cation and anion layers at approximately 0.3 nm and 0.5 nm away from the electrode surface. The double peak in the first anion layer matches the observed double step in the experimental data very well (Figure 4a). The position of the anion layers predicted by MD further from the electrode surface also show good agreement with the measured ion layer positions obtained from experiment. Comparing the experimental data with the cation density curves (Figure 4b), a layer is only detected where the first cation layer occurs whereas further away from the surface there is no measurable ion layer at the positions of the cations predicted by MD simulations. Therefore, we can conclude that the measured ion−ion spacing of 0.7 nm (Figure 1c) is formed by an ion pair, which is consistent with previous results[12−15,27,31,32]

The two maxima in the first ion layer of the ion density curves represent ions of different orientations. The first anion layer at about 0.3 nm consists of ions with a solid angle close to 90° oriented parallel to the surface (Figure 4c), whereas at 0.5 nm, the angle becomes 0 and 180° (perpendicular to the surface). The same is true for the cations (Figure 4d) which show a 0 and 180° orientation at 0.3 nm (parallel) and 90° at 0.5 nm (perpendicular). This observation suggests that it is possible to differentiate between two different ion orientations in the first ion layer closest to the electrode surface by performing AFM force spectroscopy.

Beyond this first ion layer, the cations and anions show a layered structure and the ion orientation becomes random as for the IL bulk properties. According to MD, the spacing of the anion and cation layers away from the electrode surface is primarily determined by the ion coupling and ion size whereas the distance between the electrode surface and the first ion layer is mainly determined by the ion size, orientation, and van der Waals forces between ions and electrode.

Once a bias is applied to the electrode, Coulombic interactions dominate the interaction between ions and

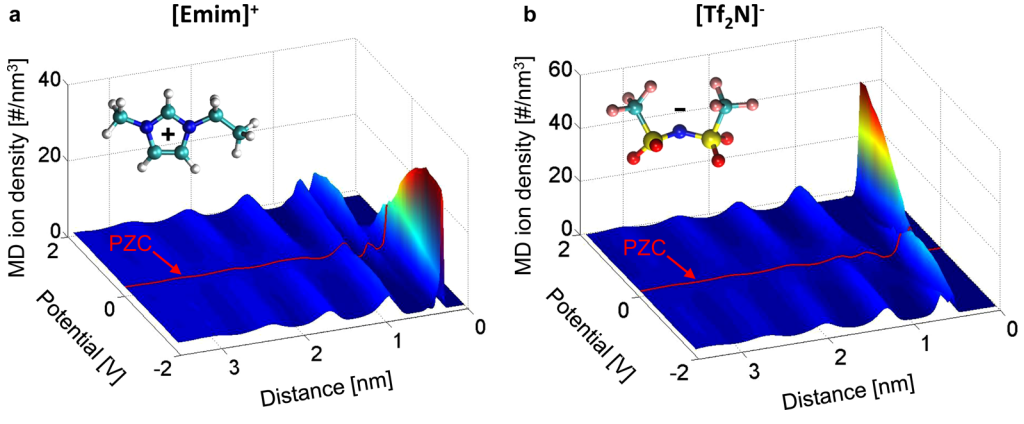

Figure 3. Cation and anion density from MD as function of applied potential. Number density profiles of cations (a) and anions (b) near the electrode surface as a function of applied potential. The potential of zero charge (PZC) is indicated as a red line.

dx.doi.org/10.1021/nl4031083 | Nano Lett. 2013, 13, 5954−5960

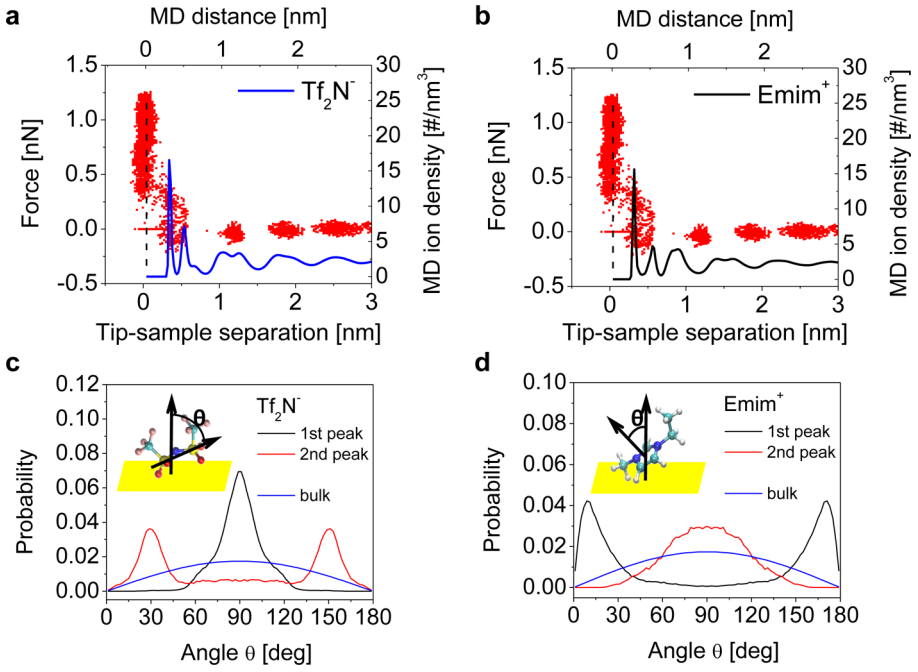

Figure 4. Comparison of experiment and MD at PZC. Comparison of the anion (a) and cation (b) MD density distribution and the experimental data from Figure 2a (>50% probability) at the PZC. Ion orientation in the first ion layer described as a double peak in the ion density distribution for anions (c) and cations (d).

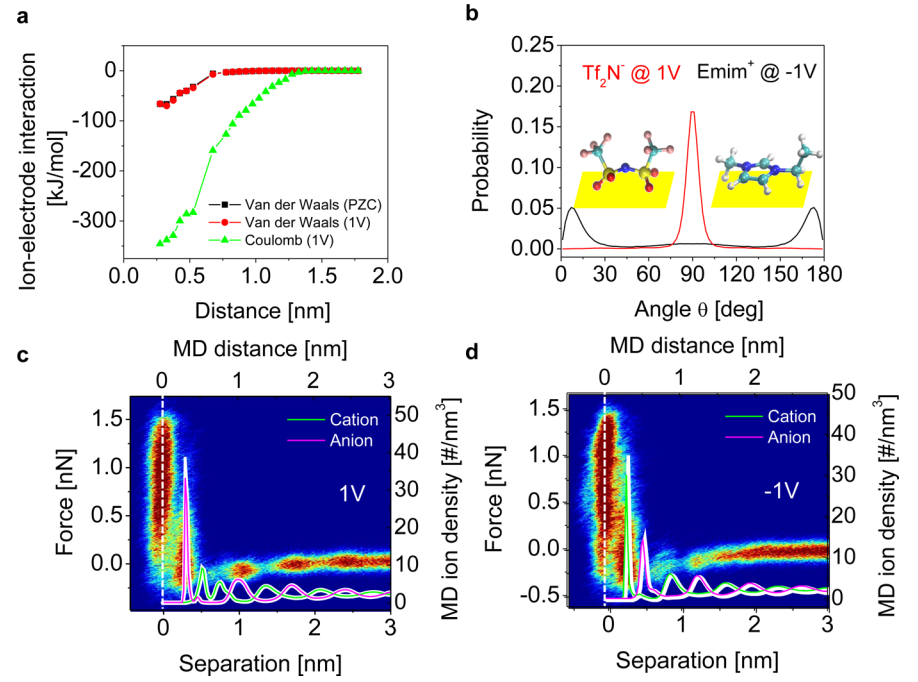

Figure 5. Comparison of experiment and MD for biased sample. (a) MD calculation of the ion−electrode interaction at PZC and 1 V bias applied to the electrode. (b) Orientation of the cation and anion layer closest to the electrode surface for −1 and 1 V, respectively (see Figure 4 for the illustration of the angle describing ion orientation). Comparison of experimental force separation curves under bias as 2D histogram with MD simulations of cation and anion positions for positive (c) and negative potentials (d). The white line denotes the position of the electrode surface.

electrode (Figure 5a), which changes the structure of the EDL. This affects mainly the very first ion layer, which contains predominantly cations for −1 V bias and anions for 1 V bias. The ions are almost oriented parallel to the electrode surface (Figure 5b) and the MD density profile shows only one peak in the near electrode region <0.6 nm. Figure 5c,d displays the comparison of the 2D histogram of the force separation curves for the biased HOPG surfaces overlaid with the simulation-predicted ion density curves for cations and anions. For the positively biased HOPG electrode (Figure 5c), the ion layer closest to the surface matches the calculated position of the first anion layer. The experimentally determined spacing from the electrode surface is 0.31 nm (Figure 2b), which matches the calculation with 0.32 nm. The following anion layer further

dx.doi.org/10.1021/nl4031083 | *Nano Lett.* 2013, 13, 5954−5960

away from the surface matches the experimental values as well. As in the unbiased case, only the anion layers are detected consistent with the ions being removed as ion pairs. For a bias of −1 V, the first layer is a cation layer that balances the negative surface charge, and force−spectroscopy measurements are able to detect this strongly bound cation layer (Figure 5d). Here, the calculated distance between electrode surface and cations is 0.29 nm versus 0.26 nm determined experimentally (Figure 2c). The distance of cations from the electrode surface at −1 V is closer than the anion layer for 1 V bias. The next ion layer measured reproducibly coincides with an anion layer position at 1.25 nm. A low-probability peak in the force spectroscopy profile appears at ca. 0.75 nm that does not correspond well to the position of the second anion layer (0.51 nm) or cation layer (0.87 nm) predicted from MD. It is possible that the presence of the AFM tip or potential ion layers surrounding the AFM tip disturb the intermediate ion layers (layers 2−3) at the HOPG surface causing a discrepancy between the MD simulations and force−spectroscopy measurements, however, this effect was not observed for the unbiased or positively biased surface. Further investigations are needed to clarify the origin of the described discrepancy.

Force distance curves were presented to measure the ion layering of $[Emim^+][Tf_2N^-]$ in the EDL on HOPG. Subnanometer ion layer spacings were extracted after statistical analysis of the force distance curves and compared with ion density calculations using MD simulations. By combining the information from the force distance curves and the MD simulation, we gain a comprehensive picture of the structure of the EDL formed at unbiased and biased HOPG electrodes. The MD simulation provides the ion density and distance between ion layers and charged surface that can be verified experimentally. This is the first time AFM force spectroscopy and MD were combined to characterize the EDL, and excellent agreement between the two methods was observed. In the future, it is desirable to perform these measurements in an electrochemically defined environment with a counter and reference electrode that will allow the comparison of ion layering and the macroscopic capacitance.

Comparison of experimental data with MD simulations allowed for the assignment of the measured ion layers to either cation or anion layers. At the PZC, the first ion layer closest to the surface consists of cations and anions in two different distinct ion orientations parallel and perpendicular to the electrode surface. Both of these molecular orientations can be detected experimentally with AFM force spectroscopy. The ion arrangement in the layer closest to the surface at ±1 V is quite different from that at PZC through the addition of Coulombic forces between ion and electrode. This results in a preferred ion orientation parallel to the electrode surface. Here, the calculated ion−electrode distance matches the distances extracted from the force distance curves. Beyond ∼1.0 nm, the charge on the electrode is almost completely screened, which implies that the charged electrode primarily affects the ions within 1.0 nm. Beyond the first ion layer, the ions show a layered structure without a preferred orientation and a characteristic anion−anion and cation−cation spacing of around 0.7 nm similar to the bulk properties of the IL. This work opens the pathway to study the EDL in electrochemically relevant systems for electrochemical capacitor applications where all aspects of the EDL can be investigated. This will help to further understand and improve charge storage mechanism for multiple applications.

Materials and Methods. *Experimental Section.* Measurements were conducted on freshly cleaved HOPG. A room-temperature ionic liquid electrolyte (1-ethyl-3methyl-imidazolium bis(trifluoromethanesulfonyl)imide ($[Emim^+][Tf_2N^-]$) was used in this study.[39]

Force distance curves were measured on a Cypher AFM from Asylum Research (Santa Barbara, CA) in a droplet of IL on HOPG. Scan rates were between 0.1 and 0.3 Hz. All experiments were done using an uncoated silicon nitride tip with a spring constant, k, of 0.38 N/m. A cable was connected to the HOPG sample to apply the electrical bias between the sample and the tip. In order to compare all curves and account for drift, the curves were aligned along the y-axis to be at zero force far away from the sample. In addition, the curves were shifted along the x-axis so that the retract branch of all force separation curves overlaid.

Simulation. The cation and anion distribution as function of potential on a carbon-based electrode was calculated using molecular dynamics (MD) simulations. The electrode was modeled by three layers of graphene sheets with an area of 4.26 × 4.18 nm^2 and a gap of 0.34 nm between each two layers. To generate the applied potential, the partial charge was uniformly distributed among the carbon atoms of two inner planar graphene sheets in contact with electrolyte. Simulations were performed in the NVT ensemble using a customized MD code based on the Gromacs software.[40] The electrolyte temperature was maintained at 300 K using the Berendsen thermostat. The electrostatic interactions were computed using the PME method.[41] Specifically, an FFT grid spacing of 0.1 nm and cubic interpolation for charge distribution were used to compute the electrostatic interactions in reciprocal space. A cutoff distance of 1.1 nm was used in the calculation of electrostatic interactions in the real space. The nonelectrostatic interactions were computed by direct summation with a cutoff length of 1.1 nm. The LINCS algorithm[42] was used to maintain bond lengths in the $Emim^+$ and Tf_2N^- ions. To reach equilibrium, the simulation was first run for 6 ns and then a 9 ns production run was performed.

The potential drop, ϕ_{EDL}, between the electrode surface and the bulk IL was obtained using our previous techniques.[43] Since the potential of zero charge (PZC) is not zero for all simulation systems, $V_{EDL} = \phi_{EDL} - PZC$ was considered as the potential applied on each EDL for convenience.[43,44] The ion number density profile was computed by binning method,[23] and the ion-electrode interaction potential was calculated based on van der Waals interaction and Coulombic interaction with a cutoff distance of 1.1 nm.[41]

AUTHOR INFORMATION

Corresponding Authors

*E-mail: (N.B.) balken@ornl.gov (experiment).
*E-mail: (G.F.) guang.feng@vanderbilt.edu (theory).

Notes

The authors declare no competing financial interest.

ACKNOWLEDGMENTS

The experimental, modeling, and sample preparation efforts of J.B., G.F., P.T.C., P.C.H., and S.D. were supported by the Fluid Interface Reactions, Structures and Transport (FIRST), an Energy Frontier Research Center funded by the U.S. Department of Energy, Office of Science, Office of Basic Energy Sciences. The experiments were performed at Asylum

Research in Santa Barbara. Additional personal support was provided by the U.S. Department of Energy, Basic Energy Sciences, Materials Sciences and Engineering Division through the Office of Science Early Career Research Program (N.B.) and the Center for Nanophase Materials Sciences, which is sponsored at Oak Ridge National Laboratory by the Scientific User Facilities Division, Office of Basic Energy Sciences, U.S. Department of Energy (S.V.K.).

REFERENCES

(1) Simon, P.; Gogotsi, Y. Materials for electrochemical capacitors. *Nat. Mater.* **2008**, *7*, 845−854.
(2) Simon, P.; Gogotsi, Y. Capacitive Energy Storage in Nanostructured Carbon−Electrolyte Systems. *Acc. Chem. Res.* **2012**, *46*, 1094−1103.
(3) Pognon, G.; Brousse, T.; Belanger, D. Effect of molecular grafting on the pore size distribution and the double layer capacitance of activated carbon for electrochemical double layer capacitors. *Carbon* **2011**, *9*, 1340−1348.
(4) Lota, G.; Grzyb, B.; Machnikowska, H.; Machnikowski, J.; Frackowiak, E. Effect of nitrogen in carbon electrode on the supercapacitor performance. *Chem. Phys. Lett.* **2005**, *404*, 53−58.
(5) Kalinathan, K.; DesRoches, D. P.; Liu, X.; Pickup, P. G. Anthraquinone modified carbon fabric supercapacitors with improved energy and power densities. *J. Power Sources* **2008**, *181*, 182−185.
(6) Fic, K.; Frackowiak, E.; Beguin, F. Unusual energy enhancement in carbon-based electrochemical capacitors. *J. Mater. Chem.* **2012**, *22*, 24213−24223.
(7) Lewandowski, A.; Olejniczak, A.; Galinski, M.; Stepniak, I. Performance of carbon−carbon supercapacitors based on organic, aqueous and ionic liquid electrolytes. *J. Power Sources* **2010**, *195*, 5814−5819.
(8) Chmiola, J.; Yushin, G.; Gogotsi, Y.; Portet, C.; Simon, P.; Taberna, P. L. Anomalous Increase in Carbon Capacitance at Pore Sizes Less Than 1 Nanometer. *Science* **2006**, *313*, 1760−1763.
(9) Chmiola, J.; Yushin, G.; Dash, R.; Gogotsi, Y. Effect of pore size and surface area of carbide derived carbons on specific capacitance. *J. Power Sources* **2006**, *158*, 765−772.
(10) Arruda, T. M.; Heon, M.; Presser, V.; Hillesheim, P. C.; Dai, S.; Gogotsi, Y.; Kalinin, S. V.; Balke, N. In situ tracking of the nanoscale expansion of porous carbon electrodes. *Energy Environ. Sci.* **2013**, *6*, 225−231.
(11) Horn, R. G.; Evans, D. F.; Ninham, B. W. Double-layer and Solvation Forces Measured in a Molten-Salt and Its Mixtures with Water. *J. Phys. Chem.* **1998**, *92*, 3531−3537.
(12) Perkin, S.; Albrecht, T.; Klein, J. Layering and shear properties of an ionic liquid, 1-ethyl-3-methylimidazolium ethylsulfate, confined to nano-films between mica surfaces. *Phys. Chem. Chem. Phys.* **2010**, *12*, 1243−1247.
(13) Perkin, S.; Crowhurst, L.; Niedermeyer, H.; Welton, T.; Smith, A. M.; Gosvami, N. N. Self-assembly in the electrical double layer of ionic liquids. *Chem. Commun.* **2011**, *47*, 6572−6574.
(14) Ueno, K.; Kasuya, M.; Watanabe, M.; Mizukami, M.; Kurihara, K. Resonance shear measurement of nanoconfined ionic liquids. *Phys. Chem. Chem. Phys.* **2010**, *12*, 4066−4071.
(15) Bou-Malham, I.; Bureau, L. Nanoconfined ionic liquids: effect of surface charges on flow and molecular layering. *Soft Mater.* **2010**, *6*, 4062−4065.
(16) Mezger, M.; Schroder, H.; Reichert, H.; Schramm, S.; Okasinski, J. S.; Schoder, S.; Honkimaki, V.; Deutsch, M.; Ocko, B. M.; Ralston, J.; Rohwerder, M.; Stratmann, M.; Dosch, H. Molecular layering of fluorinated ionic liquids at a charged sapphire (0001) surface. *Science* **2008**, *322*, 424−428.
(17) Zhou, H.; Rouha, M.; Feng, G.; Lee, S. S.; Docherty, H.; Fenter, P.; Cummings, P. T.; Fulvio, P. F.; Dai, S.; McDonough, J.; Presser, V.; Gogotsi, Y. Nanoscale Perturbations of Room Temperature Ionic Liquid Structure at Charged and Uncharged Interfaces. *ACS Nano* **2012**, *6*, 9818−9827.
(18) Fedorov, M. V.; Kornyshev, A. A. Ionic Liquid near a Charged Wall: Structure and Capacitance of Electrical Double Layer. *J. Phys. Chem. B* **2008**, *112*, 11868−11872.
(19) Sloutskin, E.; Lynden-Bell, R. M.; Balasubramanian, S.; Deutsch, M. The surface structure of ionic liquids: Comparing simulations with x-ray measurements. *J. Chem. Phys.* **2006**, 125.
(20) Lynden-Bell, R. M.; Del Pópolo, M. Simulation of the surface structure of butylmethylimidazolium ionic liquids. *Phys. Chem. Chem. Phys.* **2006**, *8*, 949−954.
(21) Wang, S.; Li, S.; Cao, Z.; Yan, T. Molecular Dynamic Simulations of Ionic Liquids at Graphite Surface. *J. Phys. Chem. C* **2010**, *114*, 990−995.
(22) Kislenko, S. A.; Amirov, R. H.; Samoylov, I. S.: Molecular dynamics simulation of the electrical double layer in ionic liquids. In *7th International Conference on Applied Electrostatics*; Li, J., Ed.; Iop Publishing Ltd: Bristol, 2013; Vol. *418*.
(23) Feng, G.; Zhang, J. S.; Qiao, R. Microstructure and Capacitance of the Electrical Double Layers at the Interface of Ionic Liquids and Planar Electrodes. *J. Phys. Chem. C* **2009**, *113*, 4549−4559.
(24) Feng, G.; Qiao, R.; Huang, J.; Dai, S.; Sumpter, B. G.; Meunier, V. The importance of ion size and electrode curvature on electrical double layers in ionic liquids. *Phys. Chem. Chem. Phys.* **2011**, *13*, 1152−1161.
(25) Zhang, X.; Zhong, Y.-X.; Yan, J.-W.; Su, Y.-Z.; Zhang, M.; Mao, B.-W. Probing double layer structures of Au (111)-BMIPF6 ionic liquid interfaces from potential-dependent AFM force curves. *Chem. Commun.* **2012**, *48*, 582−584.
(26) Atkin, R.; El Abedin, S. Z.; Hayes, R.; Gasparotto, L. H. S.; Borisenko, N.; Endres, F. AFM and STM Studies on the Surface Interaction of BMP TFSA and (EMIm TFSA Ionic Liquids with Au(111). *J. Phys. Chem. C* **2009**, *113*, 13266−13272.
(27) Hayes, R.; Warr, G. G.; Atkin, R. At the interface: solvation and designing ionic liquids. *Phys. Chem. Chem. Phys.* **2010**, *12*, 1709−1723.
(28) Hayes, R.; Borisenko, N.; Tam, M. K.; Howlett, P. C.; Endres, F.; Atkin, R. Double Layer Structure of Ionic Liquids at the Au(111) Electrode Interface: An Atomic Force Microscopy Investigation. *J. Phys. Chem. C* **2011**, *115*, 6855−6863.
(29) Atkin, R.; Borisenko, N.; Drueschler, M.; El Abedin, S. Z.; Endres, F.; Hayes, R.; Huber, B.; Roling, B. An in situ STM/AFM and impedance spectroscopy study of the extremely pure 1-butyl-1-methylpyrrolidinium tris(pentafluoroethyl) trifluorophosphate/Au(111) interface: potential dependent solvation layers and the herringbone reconstruction. *Phys. Chem. Chem. Phys.* **2011**, *13*, 6849−6857.
(30) Endres, F.; Borisenko, N.; El Abedin, S. Z.; Hayes, R.; Atkin, R. The interface ionic liquid(s)/electrode(s): In situ STM and AFM measurements. *Faraday Discuss.* **2012**, *154*, 221−233.
(31) Hayes, R.; El Abedin, S. Z.; Atkin, R. Pronounced Structure in Confined Aprotic Room-Temperature Ionic Liquids. *J. Phys. Chem. B* **2009**, *113*, 7049−7052.
(32) Atkin, R.; Warr, G. G. Structure in Confined Room-Temperature Ionic Liquids. *J. Phys. Chem. C* **2007**, *111*, 5162−5168.
(33) Labuda, A.; Grütter, P. Atomic Force Microscopy in Viscous Ionic Liquids. *Langmuir* **2012**, *28*, 5319−5322.
(34) Kaggwa, G. B.; Nalam, P. C.; Kilpatrick, J. I.; Spencer, N. D.; Jarvis, S. P. Impact of Hydrophillic/Hydrophobic Surface Chemistry on Hydration Forces in the Absence of Confinement. *Langmuir.* **2012**, *28*, 6589−6594.
(35) Argyris, D.; Ashby, P. D.; Striolo, A. Structure and Orientation of Interfacial Water Determine Atomic Force Microscopy Results: Insights from Molecular Dynamics Simulations. *ACS Nano* **2011**, *5*, 2215−2223.
(36) Gelb, L. D.; Lynden-Bell, R. M. Force oscillations and liquid structure in simulations of an atomic force microscope tip in a liquid. *Chem. Phys. Lett.* **1993**, *211*, 328−332.
(37) Gelb, L. D.; Lynden-Bell, R. M. Effects of atomic-force-microscope tip characteristics on measurement of solvation-force oscillations. *Phys. Rev. B* **1994**, *49*, 2058−2066.

(38) Patrick, D. L.; Lynden-Bell, R. M. Atomistic simulations of fluid structure and solvation forces in atomic force microscopy. *Surf. Sci.* **1997**, *380*, 224−244.
(39) Burrell, A. K.; Sesto, R. E. D.; Baker, S. N.; McCleskey, T. M.; Baker, G. A. The large scale synthesis of pure imidazolium and pyrrolidinium ionic liquids. *Green Chem.* **2007**, *9*, 449−454.
(40) Lindahl, E.; Hess, B.; van der Spoel, D. GROMACS 3.0: A package for molecular simulation and trajectory analysis. *J. Mol. Model.* **2001**, *7*, 306−317.
(41) Yeh, I. C.; Berkowitz, M. L. Ewald summation for systems with slab geometry. *J. Chem. Phys.* **1999**, *111*, 3155−3162.
(42) Hess, B.; Bekker, H.; Berendsen, H. J. C.; Fraaije, J. G. E. M. LINCS: A linear constraint solver for molecular simulations. *J. Comput. Chem.* **1997**, *18*, 1463−1472.
(43) Feng, G.; Jiang, D.; Cummings, P. T. Curvature Effect on the Capacitance of Electric Double Layers at Ionic Liquid/Onion-Like Carbon Interfaces. *J. Chem. Theory Comput.* **2012**, *8*, 1058−1063.
(44) Feng, G.; Cummings, P. T. Supercapacitor Capacitance Exhibits Oscillatory Behavior as a Function of Nanopore Size. *J. Phys. Chem. Lett.* **2011**, *2*, 2859−2864.